# Unraveling the Biomolecular Snapshots of Mitosis in Healthy and Cancer Cells Using Plasmonically-Enhanced Raman Spectroscopy

Sajanlal R. Panikkanvalappil, Steven M. Hira, Mahmoud A. Mahmoud, and Mostafa A. El-Sayed*

Laser Dynamics Laboratory, School of Chemistry and Biochemistry, Georgia Institute of Technology, Atlanta, Georgia 30332-0400, United States

S *Supporting Information*

ABSTRACT: Owing to the dynamic and complex nature of mitosis, precise and timely executions of biomolecular events are critical for high fidelity cell division. In this context, visualization of such complex events at the molecular level can provide vital information on the biomolecular processes in abnormal cells. Here, we explored the plasmonically enhanced light scattering properties of functionalized gold nanocubes (AuNCs) together with surface-enhanced Raman spectroscopy (SERS) to unravel the complex and dynamic biological processes involved in mitosis of healthy and cancerous cells from its molecular perspectives. By monitoring various stages of mitosis using SERS, we noticed that relatively high rate of conversion of mitotic proteins from their α-helix structure to β-sheet conformation is likely in the cancer cells during meta-, ana-, and telophases. Unique biochemical modifications to the lipid and amino acid moieties, associated with the observed protein conformational modifications, were also identified. However, in healthy cells, the existence of proteins in their β conformation was momentary and was largely in the α-helix form. The role of abnormal conformational modifications of mitotic proteins on the development of anomalous mitotic activities was further confirmed by looking at plasmonic nanoparticle-induced cytokinesis failure in cancer cells. Our findings illustrate the vast possibilities of SERS in real-time tracking of complex, subtle, and momentary modifications of biomolecules in live cells, which could provide new insights to the role of protein conformation dynamics during mitosis on the development of cancer and many other diseases.
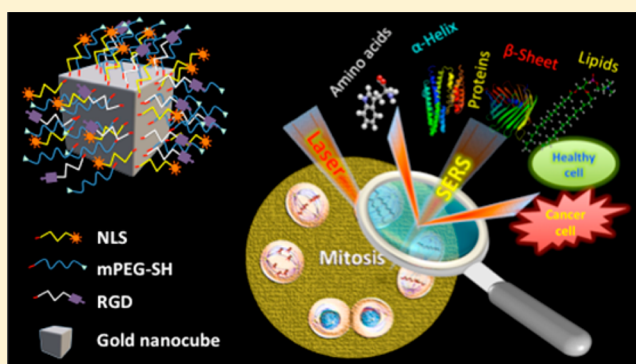
INTRODUCTION

Mitosis is a highly coordinated process, which is complex and dynamic in nature.[1] Errors in this process may lead to the formation of cells with abnormal ploidy, a hallmark of malignant cells.[2,3] Understanding various biochemical aspects of mitosis in cancer cells requires a systematic investigation of various biomolecular events associated with this process, as it can enhance our knowledge about the cancer cell responses, thereby to develop more efficient diagnostic and therapeutic techniques against cancer. Due to the dynamic nature of this process, simultaneous visualization of various chemical and conformational modifications to the biomolecules involved in mitosis is challenging. Consequently, there is a need for high-throughput methods for the precise identification of subtle and momentary mitotic errors. Though fluorescent probe-based techniques enable tracking intracellular biochemistry during mitosis,[4-6] it is still challenging to get the biochemical information on the whole process with this technique as the multitude of biomolecular modifications during cell cycle processes require specific sensors for each enzymatic target.

The excellent optical properties of the plasmonic nano-particles such as localized surface plasmon resonance and enhanced light scattering properties have been widely used for sensing and light scattering imaging of live cells.[7-10] Among various analytical techniques, Raman spectroscopy is being widely used for the investigation of living cells owing to its noninvasive nature and its advantages over other techniques as it does not require staining and is capable of providing precise chemical information on biomolecular components inside the cells via their sensitivity of vibrational bands to molecular conformation and environmental changes.[11-14] Even though Raman spectroscopy has made significant advancement in cancer diagnosis in vitro and in vivo,[15-17] attaining information on biomolecular modification associated with various biological events is still a difficult task, as only subtle changes happen during these events. On the other hand, the high signal amplification in surface-enhanced Raman scattering (SERS) has generated excitement in visualization of molecular fingerprint snapshots as well as structural and functional modifications associated with various biomolecules during biological events.[18-22] As the enhanced Raman signal comes from the immediate nano-environment around the nanoparticles in the SERS process, this method is capable of providing information

about the biomolecular composition of the region of interest inside the live cells adjacent to the nanoparticle, which cannot be expected in a conventional Raman spectroscopy. Here, in view of unraveling the cell responses in cancer and non-cancerous cells during mitosis, we explored the enhanced plasmonic scattering property of noble metal nanoparticles together with SERS to monitor the subtle modifications in the physiochemical nature of the biomolecules involved during this process in real-time. Unique biochemical modifications to the lipid and amino acid moieties, associated with the observed protein conformational modifications, were also identified. It is important to note that protein misfolding can result in failure of its normal function and subsequent development of various diseases.[23]

EXPERIMENTAL SECTION

Materials. Hydrogen tetrachloroaurate trihydrate aqueous solution ($HAuCl_4 \cdot 3H_2O$), sodium borohydride ($NaBH_4$), ascorbic acid, cetyltrimethylammonium bromide (CTAB), and trisodium citrate were purchased from Sigma-Aldrich USA. Custom-made peptides such as RGD (RGDRGDRGDRGDPGC) and NLS (CGGGPKKKRKVGG) were purchased from GenScript USA, Inc. Thiol-modified methoxypolyethylene glycol (mPEG-SH, MW 5000) was obtained from Laysan Bio, Inc.

Instrumentation. The transmission electron microscopic (TEM) images were collected using a JEOL 100CX-2 microscope. The average diameter of the nanoparticles was determined using ImageJ software. Dark-field images and SERS spectra from the human oral squamous cell carcinoma (HSC) and human keratinocyte (HaCaT) cells were collected using a Renishaw inVia Raman Microscope coupled with Leica microscope. A 785 nm diode laser was used for the SERS measurements.

Synthesis of Gold Nanocubes (~46 nm Edge Length). Gold nanocubes (AuNCs) were prepared by following the seed-mediated method reported by Murphy et al.[24] The seed nanoparticles were prepared by the reduction of 2.75 mL $HAuCl_4 \cdot 3H_2O$ (0.909 mM), which is mixed with the solution of 0.283 g of CTAB dissolved in 5 mL deionized water (DI), by 600 μL of an ice cold 0.01 M $NaBH_4$ solution under stirring for 2 min. After 1 h, 0.35 mL of 10-fold diluted seed solution was allowed to grow for 4 h in a growth solution. The growth solution was prepared by mixing CTAB solution (2.916 g in 400 mL DI water) with $HAuCl_4 \cdot 3H_2O$ solution (0.0394 g dissolved in 143 mL DI water) followed by the addition of 6 mL ascorbic acid (1 M). The resultant CTAB stabilized AuNCs were purified by centrifugation and redispersion in DI water.

Synthesis of Gold Nanospheres (~42 nm Diameter). Gold nanospheres (AuNSs) were prepared by the citrate reduction approach.[25] Briefly, 150 mL of 1% $HAuCl_4 \cdot 3H_2O$ aqueous solution was brought to boiling, and 3 mL of 0.32% trisodium citrate trihydrate was added. The solution was heated and stirred until it turned the color to red wine. The AuNSs solution was then allowed to cool down to the room temperature.

Preparation of PEG/RGD/NLS-Functionalized Gold Nanoparticles. In order to reduce the cytotoxicity of the gold nanoparticles (AuNCs or AuNSs), they were first conjugated with mPEG-SH. Here, 15 mL of 0.217 nm AuNCs was incubated with 85.7 μL of mPEG-SH (1 mM) for 24 h. For conjugating AuNSs with mPEG-SH, 10 mL of 1.596 nm AuNSs solution was treated with 29 μL of 1 mM mPEG-SH solution for 24 h. Afterward, the PEGylated nanoparticles were treated with RGD and NLS with a ratio of 4:10 to yield PEG/RGD/NLS-functionalized nanoparticles. The nanoparticles at different stages of preparation were purified by centrifugation to remove unbound ligands.

Cell Culture. HSC and HaCaT cells were cultured in Dulbecco's modified eagles' medium (DMEM, Mediatech), with phenol red, supplemented with 10% v/v fetal bovine serum (FBS, Mediatech) and 1% antimycotic solution (Mediatech) in a 37 °C, 5% CO_2 humidified incubator. For the SERS studies, the cells were grown on glass coverslips in complete growth medium at 37 °C for 24 h. Afterward, the cells were incubated with appropriate concentrations of PEG/RGD/NLS-functionalized nanoparticles (AuNCs or AuNSs), diluted in supplemented DMEM cell culture medium, for 24 h. The concentration of the nanoparticles was maintained in such a way to avoid any possible DNA damage. The cells were then synchronized in the G1 phase by serum *starvation* for 24 h as previously reported.[18] Subsequently, they were released into complete medium and grown for ~24 h before SERS experiments.

In Vitro SERS Measurements. SERS spectra were collected from the cells, which are in prometaphase or metaphase, in a time-dependent manner. Data collected from five independent experiments were analyzed in each case. The spectra were measured with a 1200 lines/mm grating using a Renishaw InVia Raman spectrometer. The laser (785 nm) was directed into a microscope via a series of reflecting lenses and apertures, where it was focused onto the sample by a 50×/0.75 N.A. objective. The backscattered signals from the samples were collected by a CCD detector in the range of 400−1800 cm^{-1} with an integration time of 10 s. The spectra were processed by removal of the spectral background. Here, cubic spline interpolation is used for the baseline fit by manually selecting the points representative of the background. Dark-field microscopic images were acquired using Lumenera's infinity2 CCD digital camera.

RESULTS AND DISCUSSION

Though mitosis is the shortest phase of the cell cycles, it is highly complex and dynamic in nature. Hence, monitoring such processes in real-time is challenging. Here, we used AuNCs for our studies owing to their high electric field distribution around its corners and edges, which is capable of enhancing the intensities of Raman vibrations to a large extent.[26] The AuNCs were synthesized by following a modified seed-mediated method (see Experimental section for details). For the cell studies, we used AuNCs, which are functionalized with methoxypolyethyelene glycol (PEG) molecules in order to minimize their cytotoxicity. Further, these particles were conjugated with RGD and NLS (peptide sequences used for enhancing the cellular uptake of the nanoparticles and targeting the nucleus, respectively) to target them toward the nucleus (Figure 1A).
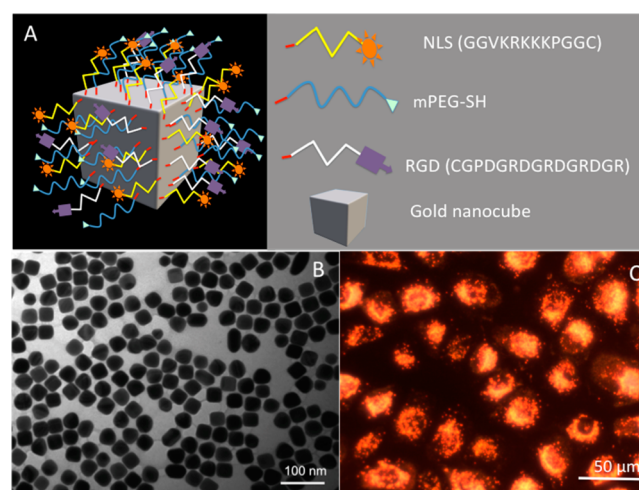

Figure 1. (A) Schematic showing the functionalized AuNC used for the study. (B) TEM image of the AuNCs. (C) DF image of the HSC cells after incubating with RGD-NLS-PEG-conjugated AuNCs. The image shows that the AuNCs are mainly localized at the nuclear region.
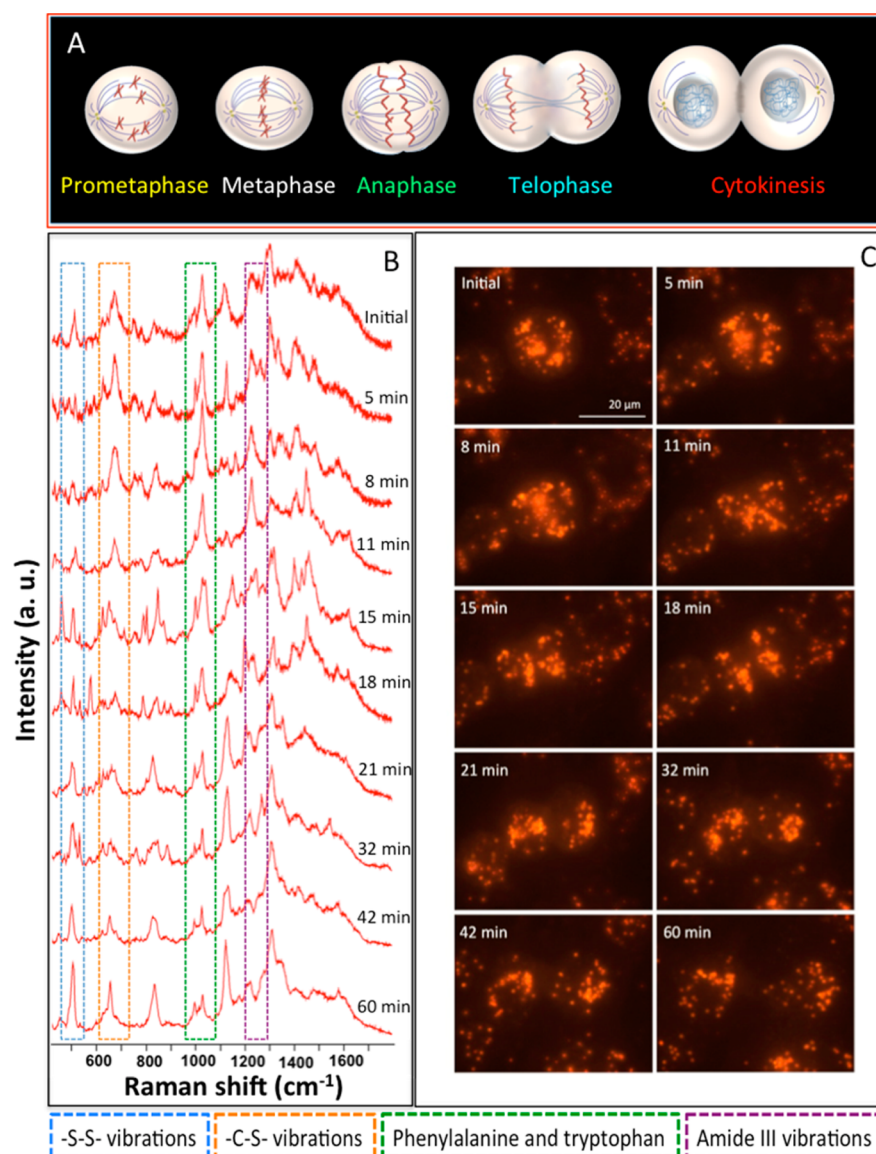
Figure 2. (A) Schematic representation of various stages of mitosis. (B) Time-dependent SERS spectra collected from the HSC cells at different stages of mitosis. DF images collected at respective time are also given (C).

The size and shape of the AuNCs were characterized by using TEM and found that they have an average edge length of ~46 nm (Figure 1B). Presence of some assorted shape along with the cubical nanoparticles was also obvious in the TEM image. The AuNCs showed an absorption maximum at ~532 nm, which is shown in Figure S1. The uptake of the AuNCs by the cancer cells (HSC) after 24 h incubation was confirmed by the dark-field (DF) microscopy, which showed the localization of AuNCs predominantly in the nuclear region of the cells (Figure 1C). The concentration of the AuNCs was maintained as low as possible (0.007 nM) to avoid any possible DNA damage. For the real-time monitoring of mitosis using SERS, AuNCs targeted cells were prepared by synchronizing them into G1 phase by serum *starvation* and subsequent release into the fresh medium. The mitotic cells in their prometaphase/metaphase were selected for the real-time study. Transition of the cells to the prometaphase was characterized by the breakdown of their nuclear envelope. Such cells were easily identifiable and appeared as "balled-up" and bright in the DF image (Figures 2, 3, 5 and supporting videos). Time-dependent

SERS spectra were collected from a specific point by focusing the laser onto the clustered AuNCs, which showed lesser movement inside the cells, at various time intervals. Spectra were collected from the same point throughout the measurements. In order to limit any damage to the cells by the possible laser-induced photothermal heating by the AuNCs, the cells were exposed to the laser only during the spectral acquisition. The mitotic cells underwent normal cell division, which was obvious in the video files. A schematic representation of various stages of mitosis is given in Figure 2A. The SERS spectra collected from a single HSC cell at various stages of mitosis and corresponding DF images are given in Figure 2B,C (time-lapse video clip created from the DF images, video S1, is given in the Supporting Information). The spectral collection was started as soon as the cell entered into the prometaphase (initial spectrum and DF image in Figure 2B). The spectrum at this stage showed prominent Raman bands, which are mainly attributed to the specific vibrations corresponding to proteins and lipids.

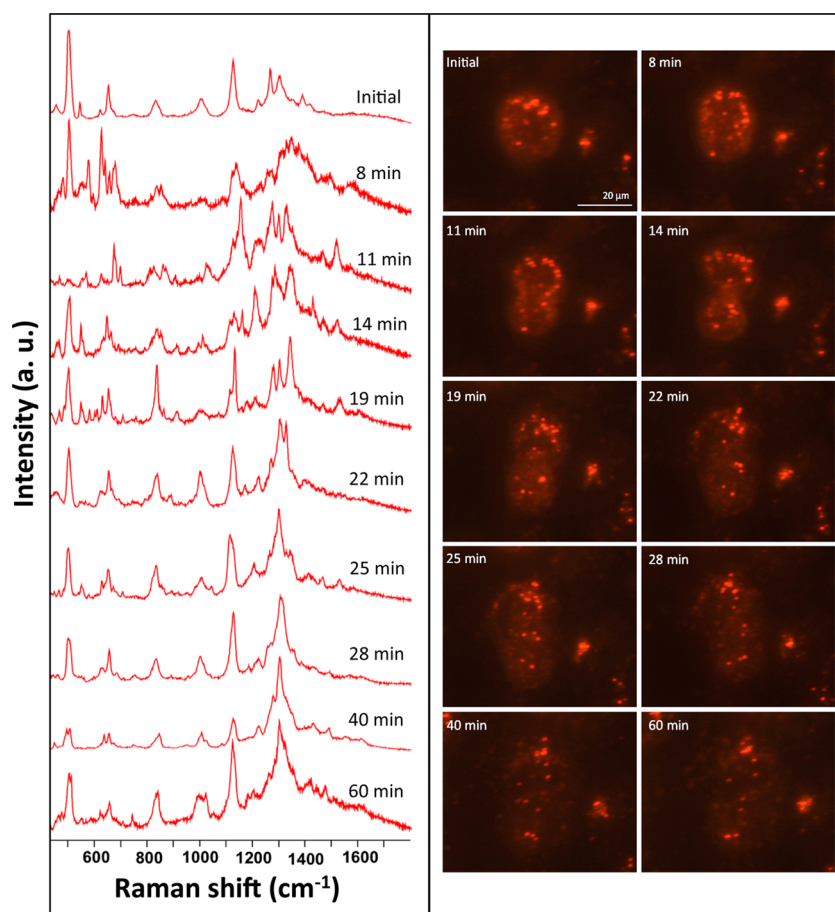The Raman bands appeared at ~502 and ~670 cm^{-1} are mainly due to the vibrations corresponding to the disulfide (S—

Figure 3. Time-dependent SERS spectra collected at different stages of mitosis in HaCaT cells. Respective DF images are also given.

Table 1. Assignment of Bands in the SERS Spectra

wavenumber (cm^{-1})	component	tentative assignments of SERS bands
495−520	protein	−S−S−
620−670	protein	−C−S− and guanine
800−850	proteins and lipid	Tyrosine in proteins and C_4N_+, O−C−C−N symmetric stretches in lipids
1000−1010	protein	RB vibration of Phe
1025−1035	protein	RB vibration of Trp and C−H in-plane bending mode of Phe
1100−1140	lipid and protein	gauche and all-*trans* conformations of lipids and C−N vibration of proteins
1210−1235	protein	amide III (*β*-pleated sheet)
1240−1255	protein	amide III (random coil)
1265−1300	protein	amide III (*α*-helix)
1300−1325	lipid	−CH$_2$ twist
1440−1460	protein and lipid	CH$_2$ bending mode of proteins and lipids along with methylene deformation

RB = ring breathing; Try = tryptophan; Phe = phenylalanine.

S) and C−S bonds of the sulfur-containing amino acids present in the mitotic proteins.[27,28] As mitosis is highly dynamic in nature, various proteins are involved in regulating this process, and these proteins will undergo conformational modifications at various stages of mitosis. Consequently, molecular environments around the AuNCs change constantly, which appear as modifications in the Raman vibration bands. The apparent change in the intensities and vibration maxima of the disulfide and C−S bands could be attributed to the possible changes in the extent of interaction between proteins and AuNCs as well as their conformational modifications and subsequent modifications in the dihedral angle of the C−S−S−C bonds.[27,29]

Because of this reason, the multiple C−S vibrations appeared in between 600 and 700 cm^{-1} regions.

In general, the amide III vibration bands of proteins are considered to be the conformational marker bands of various polypeptide backbones, which depend on the relative orientation of the N−H and C*α*-H bonds and appear as multiple bands in between 1210 and 1300 cm^{-1}.[30,31] The amide III band seen in between 1260 and 1300 cm^{-1} has been attributed to the *α*-helix structure of the proteins, whereas the spectral features found at around 1240−1255 and 1210−1235 cm^{-1} were attributed to the random coil structure and the *β*-pleated sheet conformation of the proteins, respectively. Note that C_6H_5−C stretching vibrations of phenylalanine and

tyrosine (band usually observed at 1205−1210 cm^{-1} in the normal Raman spectra)[32,33] may also contribute to the broad band corresponding to the amide III-β conformation. In the Raman spectra of HSC cell collected in the prometaphase (initial spectrum), the Raman feature corresponding to the α-helix and β-sheet conformations of amide III vibration appeared at around 1268 and 1226 cm^{-1}, respectively.

The amide III vibration corresponding to the random coil structure also appeared at around 1240 cm^{-1} as a shoulder band along with β conformational band. Among the three amide III vibrations, the Raman band at ∼1226 cm^{-1} appeared as the prominent band in the prometaphase (Figure 2B) of the mitotic HSC cells. Details on the assignments of the main vibrations in the SERS spectra are given in Table 1.

The multiple bands around 1005 and 1027 cm^{-1} are attributed to the aromatic ring breathing (RB) vibrations correspond to the amino acids such as phenylalanine (Phe) and tryptophan (Trp) (contribution from the C−H in-plane bending mode of Phe), respectively.[34−36] The Phe feature at 1005 cm^{-1} was found to be unaltered in most cases as it is unlikely to change the RB vibration of Phe with their environmental modifications and is generally used as a marker band to normalize the Raman spectra,[37] whereas the intensity of vibration of the Raman band observed at 1027 cm^{-1} was drastically modified during the course of mitosis.

The vibrational bands found in between 1100−1150 cm^{-1} of the spectral region are mainly composed of the C−C stretching vibrations of the long-chain hydrocarbon backbone of the lipid and the C−N vibration of proteins.[11,38−40] The sharp feature seen around 1110 cm^{-1} in the initial spectrum is mainly attributed to the lipid chain in their gauche conformation.[40,41] This band appeared along with a shoulder band at around 1130 cm^{-1}, which could be due to their all-trans conformation. The presence of a strong band at around 1305 cm^{-1} in the spectra also supports these arguments as lipids show a band for characteristic in-phase methylene twist in this region.[40] The vibration at ∼1450 cm^{-1} is attributed to CH$_2$ bending mode of proteins and lipids along with methylene deformation.[42]

The high sensitivity of our technique in obtaining nearly consistent spectra from a complex biological environment has been demonstrated by collecting the spectra from different cells, which were synchronized to G1 phase (Figure S3). Apart from this, SERS spectra collected from a single HSC cell (synchronized to G1 phase) at different time intervals also showed high spectral consistency (Figure S4). As mitosis is highly dynamic in nature, drastic and momentary spectral modifications are expected and were obvious in the Raman spectra. Even though large numbers of Raman bands got modified at different time intervals of mitosis, we looked at the spectral modifications to certain vibrations, which were more prominent and consistent during this process. Among the various Raman bands, vibrations correspond to S−S and C−S bonds, RB vibrations of Phe and Trp, and amide III vibrations (α-helix and β-sheet forms) showed significant and consistent changes and were studied in detail. In order to avoid any discrepancy related with the fluctuations in the intensity of the Raman signals, we studied the intensity ratio of these bands instead of their absolute intensities. The reliability of observed results was further confirmed by performing an independent experiment, where the time-dependent SERS spectra of mitosis were collected from a different HSC cell (Figure S5). The spectral trends of the aforementioned Raman bands were almost the same in both the experiments. Slight variations in

certain Raman vibrations could be due to the difference in the time intervals at which the spectra were collected.

In the SERS spectra of HSC mitosis, an obvious enhancement in the ratio between the I_{1005}/I_{1027} was observed through prometaphase to telophase (Figure 2B). The relative enhancement in the intensity of Raman RB vibration of indole ring[43] present in Trp at 1027 cm^{-1} could be attributed to the possible interaction of AuNCs with the major mitotic proteins such as microtubules and actins.[1,44] The observed Raman vibrations were in concordance with an earlier report.[45] Tubulin comprises of 2−4% of the total protein concentration in normal cells.[46] Structurally, microtubules are composed of dimerized α- and β-tubulin protein subunits. The tubulin proteins self-assemble into microtubules, and their outer surface contain several amino acids, such as histidine, methionine, and Trp that can serve as potential binding sites for gold.[47] Tubulin contains eight Trp residues at A21, A346, A388, A407, B21, B103, B346, and B407 in the two subunits[48] and are accessible for binding with AuNCs through carboxyl and indole functional groups.[49] The RB band of Trp is sensitive to the strength of the van der Waals, hydrogen bonding, and $\pi−\pi$ interactions, with surrounding amino acid residues.[50,51] The shift in the RB vibration to higher wavenumber side compared to the normal Raman vibration could be attributed to these aspects.[52] In many situations, the intensity of C−C stretching vibration of lipid backbone at 1110 cm^{-1} was inversely related to the intensity of the Trp RB vibration. The relative decrease in the intensity of vibration of lipid (1110 cm^{-1}) and simultaneous enhancement in the intensity of vibration at 1027 cm^{-1} (from prometaphase to telophase in Figure 2B) indicates the interaction of the extended hydrophobic aromatic indole ring of Trp amino acid residue and phenylalanine with lipid acyl chains.[52,53] However, the hydrophilic N−H group of the indole ring in Trp can participate in the hydrogen-bonding interaction,[54] which can result in the enhancement in the RB vibration of Trp. Moreover, Trp plays the key role in protein folding as it has the largest nonpolar surface area with polarizable indole N−H moiety.[55] Apart from this, tubulin contains 20 free cysteines (12 in α-tubulin and 8 in β-tubulin),[56] which may also take part in binding. The higher binding affinity of MTs toward AuNPs surface makes them a good template for assembling AuNPs.[45,57] As the mitosis in HSC cell progresses, the intensity of vibrations corresponding to the disulfide stretching decreased with simultaneous enhancement in the C−S vibrations. The increase in the intensity of vibration corresponds to C−S band could be due to this reason. The rapid modifications in the conformations of the mitotic proteins may also cause movements of disulfide bonds away from the nano-environment around the AuNCs. Note that the disulfide vibration usually appears at ∼502 cm^{-1} and is fairly intense in the SERS spectra of cells in their G1 phase (Figure S2). SERS spectra of HSC cell synchronized to G1 phase did not show any drastic change even after 30 min (Figure S4). Compared to G1 phase, mitotic phase is relatively short and highly dynamic. This indicates that drastic biomolecular modifications during the mitosis indeed paly an important role in the observed spectral changes.

The aforementioned observations reveal that the protein conformation has a vital role in the timely execution of mitosis. In view of studying the unique conformational modifications of proteins during mitosis, amide III vibrations (1200−1300 cm^{-1}) at various stages of mitosis were looked at in detail as these vibrations are most sensitive to protein conformations

15965

dx.doi.org/10.1021/ja506289u | J. Am. Chem. Soc. 2014, 136, 15961−15968
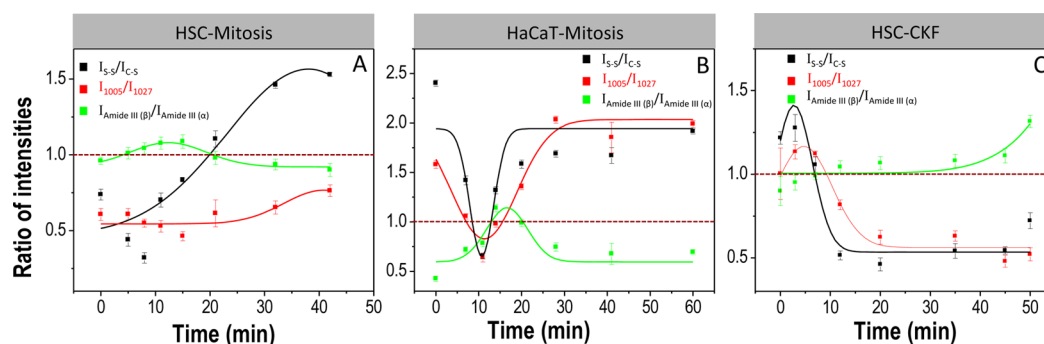
Figure 4. Plots showing variations in the ratio of intensities versus time for disulfide and C−S vibrations, ring vibrations of Phe and Trp, and amide III vibrations of β and α conformations during mitosis in HSC (A) and HaCaT (B) cells and cytokinesis failure in HSC cells (C).
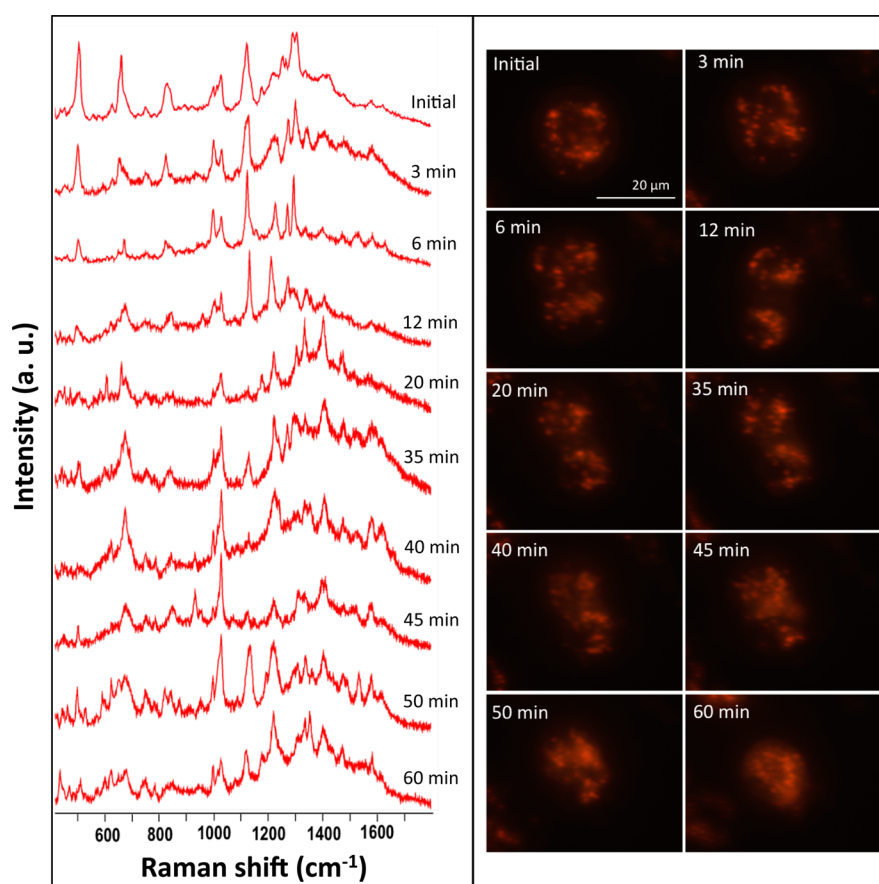

Figure 5. Time-dependent SERS spectra collected at different stages of cytokinesis failure in HSC cells. Respective DF images are also shown.

due to coupling of this vibration with Cα-H bending and C−N stretching vibrations.[58,59] It was noted that the mitotic proteins acquire β conformation as the mitosis progresses from prometaphase to telophase (Figure 2B). In comparison with the amide III vibration corresponding to the α-helix conformation (1275 cm^{-1}), a gradual increase in the vibration corresponding to β-pleated sheet (1226 cm^{-1}) was observed until telophase (18 min). As a result of conformational modification, the vibrations found at 1455 cm^{-1} of the CH$_2$ bending vibration of proteins and lipids along with methylene deformation also showed a simultaneous enhancement in its intensity. After the telophase (~18 min), the spectra collected from the daughter cells showed more resemblance to the cells in their G1 phase (Figure S2). Gradual enhancements in the vibrations correspond to the disulfide bond, lipid backbone as

well as protein C−N, lipid CH$_2$ twist and amide III vibration of α-helix conformation, were obvious in the spectra of cells after cytokinesis.

It is well-known that protein folding plays a vital role in regulation of cellular growth and differentiation.[60,61] The abnormal formation of β-sheet conformation can result in the exposure of hydrophobic amino acid residues, which may be an indication of abnormal behavior of the cells.[61] In view of identifying the unique biomolecular events associated with mitosis in cancer and healthy cells, we looked at the various stages of mitosis in healthy cells (human karatinocyte (HaCaT)), from its molecular perspective using SERS. Figure 3 shows the time-dependent SERS spectra and corresponding DF images collected from a single mitotic HaCaT cell at various stages of mitosis (also see Supporting Information

video S2). The extent of uptake of AuNCs was relatively higher in the HSC cells than in the HaCaT cells, as the HSC cell has $\alpha\beta$ integrins overexpressed on its cell surface and RGD present on the AuNC surface can effectively target them on the cancer cell surface than HaCaT cells, making AuNCs enter the cytoplasm via receptor-mediated endocytosis.[62,63] However, the amount of AuNCs endocytosed into the mitotic HaCaT cells was sufficient to get reliable SERS spectra with good intensities. Even though some of the SERS spectral features in mitotic HaCaT cells showed similar spectral trend as in HSC cells, they showed a noticeable difference in their molecular dynamics. The ratios of intensities of Raman vibrations between disulfide and C−S (I_{S-S}/I_{C-S}) vibrations, RB vibrations of Phe and Trp (I_{1005}/I_{1027}), and amide III-β and amide III-α conformations ($I_{AmideIII\,(\beta)}/I_{AmideIII\,(\alpha)}$) in HSC and HaCaT cells are plotted versus time and are given in Figure 4A,B. Spectra were collected from five independent experiments in each cases, and the intensity ratios at different time intervals were averaged (also see Figures S5 and S6 for the Raman spectra and respective DF images collected from independent experiments in each case). On the contrary to HSC cell mitosis, the existence of mitotic proteins in their β conformation was momentary in HaCaT cells. The proteins were mostly in α-helix conformation, and the intensity ratio ($I_{AmideIII\,(\beta)}/I_{AmideIII\,(\alpha)}$) was always <1 for HaCaT cells.

Dominance of β conformation was only observed during late anaphase (~11 min) and telophase (~14 min) (Figure 3), whereas in HSC cells, the mitotic proteins were in β conformation from metaphase to telophase (5−18 min) (Figures 2 and 4). As a result of the momentary transformation in protein conformation, the modifications in the disulfide and Trp vibrations were also transitory in mitotic HaCaT cells. Most of the time, the I_{S-S}/I_{C-S} and I_{1005}/I_{1027} ratios maintained a value >1 (Figure 4). The above results suggest the obvious protein conformational modification of mitotic proteins in HSC cell. As the microtubules are the main mitotic proteins, which are mainly attributed to the observed spectral modifications during the mitosis, similar kinds of spectral modifications were expected for both HSC and HaCaT cells. However, the observed results pointing toward the fact that abnormal conformational modifications of mitotic proteins to the β form during the mitosis in HSC cells result in the exposure of amino acids, which are likely to be more accessible for binding with AuNC surface.

In order to study the role of microtubules on the observed conformational modifications in the SERS spectra, biomolecular snapshots involved during gold nanoparticle-induced cytokinesis failure (CKF) in HSC cells were probed using time-dependent SERS (Figures 5 and S7). For this study, the HSC cells were incubated with 0.03 nM AuNSs. These AuNSs showed an absorption maximum around 540 nm and were ~42 nm in diameter. The extinction spectrum and TEM image of AuNSs are shown in Figure S8. It was also noted that AuNCs and AuNSs yield almost the same SERS spectra for the cells at G1 phase (Figure S2). Our early study shows that AuNSs have the potential to arrest the cytokinesis in HSC cells in nanomolar concentration range,[62] which can induce DNA damage and apoptosis. The spectral modifications during CKF (Figure 5) were almost similar as in the case of mitosis in HSC cells (Figure 2B). Nevertheless, the Raman vibration corresponding to the RB mode of Trp (1027 cm^{-1}), amide III vibration of β conformation, and C−S remained almost unaltered in their intensities during the cytokinesis process after

metaphase (Figures 4C and 5). This suggests that, apart from DNA damage, higher concentration of AuNSs most likely stabilizes the microtubules, perturbs the spindle microtubule dynamics, and leads to failure of cytokinesis.[64,65] It has been shown that stabilization of microtubules by the action of certain anticancer drugs can induce mitotic arrest in cancer cells.[6,64] DF images suggest that stabilization of microtubules blocks the ingression of the cleavage furrow resulting in cytokinesis failure (Figure 5 and Supporting Information video S3).

Overall results suggest that DF microscopy together with SERS is capable of providing the momentary and subtle biomolecular events as well as the errors in extremely complex and dynamic biological processes such as mitosis. Moreover, unique capabilities of this approach in simultaneous visualization of physical and chemical aspects of biomolecules involved in mitosis could provide new insights into the role of conformational modifications of mitotic proteins in the development of cancer cells.

CONCLUSION

Biological snapshots of various stages of mitosis in cancer and healthy cells were probed using SERS. DF microscopy together with SERS provided new insights into the chemical and conformational modifications of the proteins and lipids involved in mitosis. Unique biochemical modifications occurring in cancer cells in comparison with healthy cells were identified. Our studies suggest that the residence time of mitotic proteins in their β-sheet conformation is likely to be longer in cancer cells. Stabilization of β conformation during nanoparticle-induced cytokinesis failure also suggests that the residence time of mitotic proteins in their β conformation increases, as there are errors in mitosis. Our findings establish the vast possibilities of plasmonically enhanced Raman spectroscopy in real-time tracking of subtle cellular modifications, which could provide new insights about the role of protein conformation dynamics during mitosis in the development of cancer and many other diseases.

ASSOCIATED CONTENT

Supporting Information

TEM images and UV−vis extinction spectra of AuNCs and AuNSs; additional SERS spectra collected from different cells in their G1 phase, mitosis, and cytokinesis failure; video files showing mitosis in HSC, HaCaT cells and cytokinesis failure. This material is available free of charge via the Internet at http://pubs.acs.org.

AUTHOR INFORMATION

Corresponding Author

melsayed@gatech.edu

Notes

The authors declare no competing financial interest.

ACKNOWLEDGMENTS

REFERENCES

(1) Walczak, C. E.; Cai, S.; Khodjakov, A. *Nat. Rev. Mol. Cell Biol.* **2010**, *11*, 91.

(2) Holland, A. J.; Cleveland, D. W. *Nat. Rev. Mol. Cell Biol.* **2009**, *10*, 478.

(3) Schvartzman, J.-M.; Sotillo, R.; Benezra, R. *Nat. Rev. Cancer* **2010**, *10*, 102.

(4) Rieder, C. L.; Khodjakov, A. *Science* **2003**, *300*, 91.

(5) Zhang, J.; Campbell, R. E.; Ting, A. Y.; Tsien, R. Y. *Nat. Rev. Mol. Cell Biol.* **2002**, *3*, 906.

(6) Jones, J. T.; Myers, J. W.; Ferrell, J. E.; Meyer, T. *Nat. Biotechnol.* **2004**, *22*, 306.

(7) Qian, W.; Huang, X.; Kang, B.; El-Sayed, M. A. *J. Biomed. Opt.* **2010**, *15*, 046025.

(8) Jun, Y.-w.; Sheikholeslami, S.; Hostetter, D. R.; Tajon, C.; Craik, C. S.; Alivisatos, A. P. *Proc. Natl. Acad. Sci. U. S. A.* **2009**, *106*, 17735.

(9) Rong, G.; Wang, H.; Skewis, L. R.; Reinhard, B. r. M. *Nano Lett.* **2008**, *8*, 3386.

(10) Ali, M. R. K.; Panikkanvalappil, S. R.; El-Sayed, M. A. *J. Am. Chem. Soc.* **2014**, *136*, 4464.

(11) Puppels, G. J.; de Mul, F. F. M.; Otto, C.; Greve, J.; Robert-Nicoud, M.; Arndt-Jovin, D. J.; Jovin, T. M. *Nature* **1990**, *347*, 301.

(12) Thomas, G. J.; Prescott, B.; Olins, D. E. *Science* **1977**, *197*, 385.

(13) Harada, I.; Takeuchi, H. Raman and ultraviolet resonance Raman spectra of proteins and related compounds. In *Spectroscopy of Biological Systems, Advances in Spectroscopy*; Clark, R. J. H., Hester, R. E., Eds.; John Wiley & Sons: Chichester, UK, 1986; p 113.

(14) Barman, I.; Dingari, N. C.; Saha, A.; McGee, S.; Galindo, L. H.; Liu, W.; Plecha, D.; Klein, N.; Dasari, R. R.; Fitzmaurice, M. *Cancer Res.* **2013**, *73*, 3206.

(15) Matthäus, C.; Boydston-White, S.; Miljkovi; Milo; Romeo, M.; Diem, M. *Appl. Spectrosc.* **2006**, *60*, 1.

(16) Haka, A. S.; Shafer-Peltier, K. E.; Fitzmaurice, M.; Crowe, J.; Dasari, R. R.; Feld, M. S. *Proc. Natl. Acad. Sci. U. S. A.* **2005**, *102*, 12371.

(17) Kong, K.; Rowlands, C. J.; Varma, S.; Perkins, W.; Leach, I. H.; Koloydenko, A. A.; Williams, H. C.; Notingher, I. *Proc. Natl. Acad. Sci. U. S. A.* **2013**, *110*, 15189.

(18) Kang, B.; Austin, L. A.; El-Sayed, M. A. *Nano Lett.* **2012**, *12*, 5369.

(19) Panikkanvalappil, S. R.; Mackey, M. A.; El-Sayed, M. A. *J. Am. Chem. Soc.* **2013**, *135*, 4815.

(20) Panikkanvalappil, S. R.; Mahmoud, M. A.; Mackey, M. A.; El-Sayed, M. A. *ACS Nano* **2013**, *7*, 7524.

(21) Lyandres, O.; Glucksberg, M. R.; Walsh, J. T.; Shah, N. C.; Yonzon, C. R.; Zhang, X.; Van Duyne, R. P. In *Biomedical Vibrational Spectroscopy*; John Wiley & Sons, Inc.: Hoboken, NJ, 2007; p 221.

(22) Ahijado-Guzmán, R.; Gómez-Puertas, P.; Alvarez-Puebla, R. A.; Rivas, G.; Liz-Marzán, L. M. *ACS Nano* **2012**, *6*, 7514.

(23) Dobson, C. M. *Trends Biochem. Sci.* **1999**, *24*, 329.

(24) Sisco, P. N.; Murphy, C. J. *J. Phys. Chem. A* **2009**, *113*, 3973.

(25) Freund, P. L.; Spiro, M. *J. Phys. Chem.* **1985**, *89*, 1074.

(26) Kim, D.-S.; Heo, J.; Ahn, S.-H.; Han, S. W.; Yun, W. S.; Kim, Z. H. *Nano Lett.* **2009**, *9*, 3619.

(27) Van Wart, H. E.; Lewis, A.; Scheraga, H. A.; Saeva, F. D. *Proc. Natl. Acad. Sci. U. S. A.* **1973**, *70*, 2619.

(28) Van Wart, H. E.; Scheraga, H. A. *J. Phys. Chem.* **1976**, *80*, 1823.

(29) Chen, M. C.; Lord, R. C. *J. Am. Chem. Soc.* **1976**, *98*, 990.

(30) Maiti, N. C.; Apetri, M. M.; Zagorski, M. G.; Carey, P. R.; Anderson, V. E. *J. Am. Chem. Soc.* **2004**, *126*, 2399.

(31) Spiro, T. G. *Biological applications of Raman spectroscopy*; Wiley: Hoboken, NJ, 1987.

(32) Fodor, S. P. A.; Copeland, R. A.; Grygon, C. A.; Spiro, T. G. *J. Am. Chem. Soc.* **1989**, *111*, 5509.

(33) Asher, S. A.; Ludwig, M.; Johnson, C. R. *J. Am. Chem. Soc.* **1986**, *108*, 3186.

(34) De Gelder, J.; De Gussem, K.; Vandenabeele, P.; Moens, L. *J. Raman Spectrosc.* **2007**, *38*, 1133.

(35) Rava, R. P.; Spiro, T. G. *J. Phys. Chem.* **1985**, *89*, 1856.

(36) Fischer, W. B.; Eysel, H. H. *Spectrochim. Acta, Part A* **1992**, *48*, 725.

(37) Li, T.; Chen, Z.; Johnson, J. E.; Thomas, G. J. *Biochemistry* **1990**, *29*, 5018.

(38) Ichimura, T.; Chiu, L.-d.; Fujita, K.; Kawata, S.; Watanabe, T. M.; Yanagida, T.; Fujita, H. *PLoS One* **2014**, *9*, e84478.

(39) Rygula, A.; Majzner, K.; Marzec, K. M.; Kaczor, A.; Pilarczyk, M.; Baranska, M. *J. Raman Spectrosc.* **2013**, *44*, 1061.

(40) Lippert, J. L.; Peticolas, W. L. *Proc. Natl. Acad. Sci. U. S. A.* **1971**, *68*, 1572.

(41) Wu, H.; Volponi, J. V.; Oliver, A. E.; Parikh, A. N.; Simmons, B. A.; Singh, S. *Proc. Natl. Acad. Sci. U. S. A.* **2011**, *108*, 3809.

(42) Rehman, I. u.; Movasaghi, Z.; Rehman, S. *Vibrational spectroscopy for tissue analysis*; CRC Press: Boca Raton, FL, 2013.

(43) Chuang, C.-H.; Chen, Y.-T. *J. Raman Spectrosc.* **2009**, *40*, 150.

(44) Robinson, D. N.; Spudich, J. A. *Trends Cell Biol.* **2000**, *10*, 228.

(45) Zhou, J. C.; Wang, X.; Xue, M.; Xu, Z.; Hamasaki, T.; Yang, Y.; Wang, K.; Dunn, B. *Mater. Sci. Eng., C* **2010**, *30*, 20.

(46) Anderson, P. J. *J. Biol. Chem.* **1979**, *254*, 2168.

(47) Nogales, E.; Whittaker, M.; Milligan, R. A.; Downing, K. H. *Cell* **1999**, *96*, 79.

(48) Sardar, P. S.; Maity, S. S.; Das, L.; Ghosh, S. *Biochemistry* **2007**, *46*, 14544.

(49) Joshi, P.; Shewale, V.; Pandey, R.; Shanker, V.; Hussain, S.; Karna, S. P. *J. Phys. Chem. C* **2011**, *115*, 22818.

(50) Chi, Z.; Asher, S. A. *J. Phys. Chem. B* **1998**, *102*, 9595.

(51) Schlamadinger, D. E.; Gable, J. E.; Kim, J. E. *J. Phys. Chem. B* **2009**, *113*, 14769.

(52) Rodgers, K. R.; Su, C.; Subramaniam, S.; Spiro, T. G. *J. Am. Chem. Soc.* **1992**, *114*, 3697.

(53) Sanchez, Katheryn M.; Kang, G.; Wu, B.; Kim, Judy E. *Biophys. J.* **2011**, *100*, 2121.

(54) Dorigo, A. E.; Anderson, D. G.; Busath, D. D. *Biophys. J.* **1999**, *76*, 1897.

(55) Gallivan, J. P.; Dougherty, D. A. *Proc. Natl. Acad. Sci. U. S. A.* **1999**, *96*, 9459.

(56) Britto, P. J.; Knipling, L.; McPhie, P.; Wolff, J. *Biochem. J.* **2005**, *389*, 549.

(57) Rehman, A.; Raza, Z. A.; Saif ur, R.; Khalid, Z. M.; Subramani, C.; Rotello, V. M.; Hussain, I. *J. Colloid Interface Sci.* **2010**, *347*, 332.

(58) Asher, S. A.; Ianoul, A.; Mix, G.; Boyden, M. N.; Karnoup, A.; Diem, M.; Schweitzer-Stenner, R. *J. Am. Chem. Soc.* **2001**, *123*, 11775.

(59) Oladepo, S. A.; Xiong, K.; Hong, Z.; Asher, S. A. *J. Phys. Chem. Lett.* **2011**, *2*, 334.

(60) Radford, S. E.; Dobson, C. M. *Cell* **1999**, *97*, 291.

(61) Dobson, C. M. *Nature* **2003**, *426*, 884.

(62) Kang, B.; Mackey, M. A.; El-Sayed, M. A. *J. Am. Chem. Soc.* **2010**, *132*, 1517.

(63) Xue, H.; Atakilit, A.; Zhu, W.; Li, X.; Ramos, D. M.; Pytela, R. *Biochem. Biophys. Res. Commun.* **2001**, *288*, 610.

(64) Jordan, M. A.; Toso, R. J.; Thrower, D.; Wilson, L. *Proc. Natl. Acad. Sci. U. S. A.* **1993**, *90*, 9552.

(65) Choudhury, D.; Xavier, P. L.; Chaudhari, K.; John, R.; Dasgupta, A. K.; Pradeep, T.; Chakrabarti, G. *Nanoscale* **2013**, *5*, 4476.